Journal of Power Sources 196 (2011) 4943–4949

Contents lists available at ScienceDirect

Journal of Power Sources

journal homepage: www.elsevier.com/locate/jpowsour

Bulk conduction and relaxation in $[(ZrO_2)_{1-x}(CeO_2)_x]_{0.92}(Y_2O_3)_{0.08}$ $(0 \le x \le 1)$ solid solutions at intermediate temperatures

Fan Yang, Xiaofeng Zhao, Ping Xiao*

Materials Science Centre, School of Materials, University of Manchester, M1 7HS, UK

ARTICLE INFO

Article history:
Received 25 October 2010
Received in revised form 18 January 2011
Accepted 2 February 2011
Available online 12 February 2011

Keywords:
ZrO_2–CeO_2–Y_2O_3 solid solutions
Ionic conduction
Oxygen vacancy
Impedance spectroscopy

ABSTRACT

Bulk conduction and relaxation of the $[(ZrO_2)_{1-x}(CeO_2)_x]_{0.92}(Y_2O_3)_{0.08}$ $(0 \le x \le 1)$ solid solutions were studied using impedance spectroscopy at intermediate temperatures (200–500 °C). The bulk conductivity as a function of x shows a "V-shape" variation which is a competitive effect of the defect associates and the lattice parameter. In the ZrO_2-rich region ($x < 0.5$) CeO_2 doping increases the concentration of defect associates which limits the mobility of the oxygen vacancies; in the CeO_2-rich region ($x > 0.5$) the increase of x increases the lattice parameter which enlarges the free channel for oxygen vacancy migration. Further analysis indicates the ionic radius of the tetravalent dopant determines the composition dependence of the ionic conductivity of the solid solutions. When doping YSZ with other tetravalent dopant with similar ionic radius with Zr^{4+}, e.g., Hf^{4+}, such "V-shape" composition dependence of the bulk conductivity cannot be observed.

1. Introduction

Oxide ion conductors with cubic fluorite structure are important electrolyte materials for solid oxide fuel cells (SOFCs) [1,2], oxygen sensors [3] and oxygen pumps [4]. High ionic conductivity is achieved in such a structure when the host cations are replaced by lower valence cations, which generates oxygen ion vacancies to compensate the charge missing and to act as charge carriers [5]. The oxygen ions overcome an energy barrier to hop to neighbouring vacant sites and move diffusively to fulfil long-range transport in the material [6].

Among numerous oxide ion conductors, ZrO_2- and CeO_2-based ceramic attract the most interest and have been extensively studied [7–15]. They possess many unique physical properties which make them promising materials for practical or potential application in technologically important devices. For example, yttria-stabilized zirconia (YSZ) is the conventionally employed electrolyte material in SOFCs because of its good mechanical, chemical and electrolytic properties [16]. Doped-ceria has higher ionic conductivity, good thermodynamic stability [17] and good catalytic activity [18], therefore it is a prime candidate for the intermediate temperature SOFCs.

The ZrO_2–CeO_2–Y_2O_3 ternary solid solution which keeps the cubic fluorite structure is also a material of interest both from the practical side and the fundamental side. From the practical side, the idea of a double-layer electrolyte with YSZ on the anode side and doped CeO_2 on the cathode side has been proposed for SOFC [19,20]. The double-layer electrolyte combines the advantages of YSZ and CeO_2: it suppresses the electronic conduction caused by the reduction of Ce^{4+} at the anode side and retains the high ionic conductivity of doped-CeO_2 [21]. However, the reaction of ZrO_2 and CeO_2 leads to the formation of the ZrO_2–CeO_2–Y_2O_3 ternary solid solution between the two layers. Therefore, an investigation of the ionic conductivity of the ternary solid solution is necessary. On the fundamental side, it is a system to study the homovalent doping effect on the ionic conductivity of the solid solutions if the concentration of Y_2O_3 is constant.

Several studies on the electrical properties of the ZrO_2–CeO_2–Y_2O_3 solid solutions have been reported. However, most of the studies are focused on the mixed conduction of the solid solutions caused by the reduction of Ce^{4+} to Ce^{3+} at various oxygen partial pressures and at high temperatures (>800 °C). For example, Cales and Baumard [22] studied the total conductivity of the ternary solid solutions in a large range of oxygen partial pressures from 1000 to 1400 °C. They discussed the mixed conduction and the defect structure caused by the reduction of Ce^{4+} to Ce^{3+}, and determined the concentrations of the various charge carriers by thermogravimetry and the measurement of the magnetic susceptibility. Arashi et al. [23] studied the electrical conduction of the ZrO_2–CeO_2–Y_2O_3 solid solutions at even higher temperatures (>1200 °C). They employed the electron blocking method to separate the ionic and electronic conductivities and found that the reduction of Ce^{4+} to Ce^{3+} not only influences the relationship between ionic conductivity and

* Corresponding author. Tel.: +44 161 3065941; fax: +44 161 3063586.
E-mail address: ping.xiao@manchester.ac.uk (P. Xiao).

0378-7753/$ – see front matter © 2011 Elsevier B.V. All rights reserved.
doi:10.1016/j.jpowsour.2011.02.010

the oxygen partial pressure, but also influences the electronic contribution to the total conductivity. Ananthapadmanabhan et al. [24] studied the composition dependence of the electrical conductivity in $[(ZrO_2)_{1-x}(CeO_2)_x]_{0.9}(Y_2O_3)_{0.1}$ solid solutions from ~700 to 1300 °C in air and they proposed a simple model for the oxygen path length to explain the observed composition dependence of the conductivity.

The reduction of Ce^{4+} at high temperatures makes the ZrO_2–CeO_2–Y_2O_3 solid solution a complicated system to study the effect of tetravalent doping on the ionic conductivity. On the other hand, most of the current studies on the electrical properties of the ZrO_2–CeO_2–Y_2O_3 solid solutions were studied by DC four-probe measurement. The conductivity obtained from the dc measurement is an overall conductivity from both grain (bulk) and grain boundary. In polycrystalline ceramic materials, the grain boundary has a large influence on the electrical conductivity because of impurity segregations or the space charge effect [25]. For studying the intrinsic property of the ternary solid solution, the contribution of grain boundary to the overall conductivity should be excluded.

Therefore, in this paper, the electrical properties of the $[(ZrO_2)_{1-x}(CeO_2)_x]_{0.92}(Y_2O_3)_{0.08}$ $(0 \le x \le 1)$ were studied in an intermediate temperature range (200–500 °C) by impedance spectroscopy. The relative low temperatures were chosen to avoid the reduction of Ce^{4+} and to ensure the electrical conduction in the solid solutions is purely ionic. Impedance spectroscopy was employed to separate the bulk and the grain boundary contributions to the electrical conductivity. The purpose of this work is to study the effect of homovalent doping on the ionic conductivity of the solid solutions.

2. Experiment

The samples, formulated as $[(ZrO_2)_{1-x}(CeO_2)_x]_{0.92}(Y_2O_3)_{0.08}$ $(0 \le x \le 1)$, were synthesized by a solid state reaction method. ZrO_2 (99.6%, PI-KEM, UK), Y_2O_3 (99.99%, PI-KEM, UK) and CeO_2 (99.95%, PI-KEM, UK) powders were used as the starting materials. Appropriate amount of each powders were weighed, mixed and ball-milled in 2-propanol for 24 h using zirconia balls as grinding media. The resulting mixtures were subsequently dried in air overnight, and then ground by mortar and pestle and passed through a 45 micro sieve. The final mixtures were cold pressed into tablets under a uniaxial pressure of 100 MPa and then sintered at 1500 °C for 10 h in air. The other series of solid solutions, formulated as $[(ZrO_2)_{1-x}(HfO_2)_x]_{0.87}(Y_2O_3)_{0.13}$ $(0 \le x \le 0.8)$, were synthesized by the same powder mixing method, and sintered at 1600 °C for 4 h.

Phase compositions of the solid solutions were identified by X-ray diffraction (XRD, Philips X'Pert) method using Cu K_α radiation. The measurements were performed on the sample surfaces with a step scanning mode (step size of 0.05°) at a rage of 0.1 min^{-1}. The densities of the sintered specimens were measured by Archimedes' method. The porosities of all the samples are within 10%. Microstructures of the samples were observed by scanning electron microscope (SEM, Philips XL30). The grain sizes of the samples were estimated from the SEM images, and they were found to be around 10 μm for all the compositions.

Electrical properties of the solid solutions were obtained from ac impedance spectroscopy measurements using a Solatron SI 1255 HF frequency response analyser coupled with a Solatron 1296 Delectric Interface (Solartron, UK). Silver paint was coated on the polished surfaces of the samples and fired at 500 °C for 1 h in air to serve as electrodes. During impedance measurements, an ac voltage of 0.1 V was applied to the sample over a frequency range from 0.1 to 10^7 Hz at various temperatures. Equivalent circuit fittings of the measured impedance spectra were carried out using Zview Impedance Analysis software (Scribner Associates, Inc., Southern Pines, NC). For comparison convenience, all the impedance spectra were normalized by a geometric factor $\alpha = 4t/\pi D^2$, where t and D denote to sample thickness and diameter, respectively.

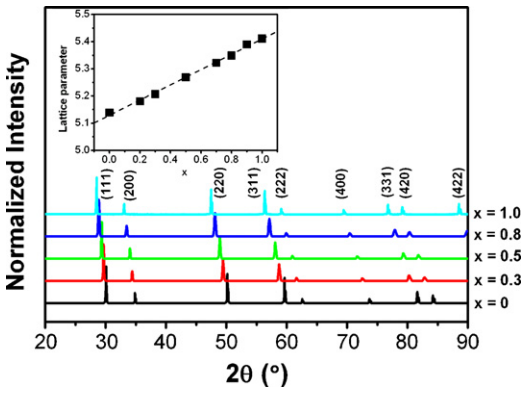

Fig. 1. X-ray diffraction patterns of the solid solutions. The inset is the lattice parameter as a function of the mole ratio of CeO_2 (x) in $[(ZrO_2)_{1-x}(CeO_2)_x]_{0.92}(Y_2O_3)_{0.08}$.

3. Results

3.1. Phase composition and lattice parameter

Fig. 1 shows the X-ray diffraction patterns of the solid solutions, which confirms that all the samples are single phase with cubic structure. The lattice parameters of the samples are shown in the inset of Fig. 1, where linear relationship between the lattice parameter and the mole ratio of CeO_2 can be observed, indicating it follows the Vegard's rule for solid solutions.

3.2. Typical impedance spectra of the solid solutions

First of all, one composition of the solid solutions $[(ZrO_2)_{0.6}(CeO_2)_{0.4}]_{0.92}(Y_2O_3)_{0.08}$ ($x = 0.4$) was selected to present the typical ac impedance behaviours of the solid solutions. Fig. 2 shows typical impedance spectra (Nyquist plots) of the solid solutions at various temperatures. Similar to the well-known impedance spectroscopy of YSZ, two semicircles are displayed on the Nyquist plot of the solid solution, from left to right (high frequency to low frequency), representing the response from grain (bulk) and grain boundary, respectively. The measured impedance spectra can be fitted by an equivalent circuit of two parallel-aligned resistance-constant phase element (R-CPE) in series connection, as

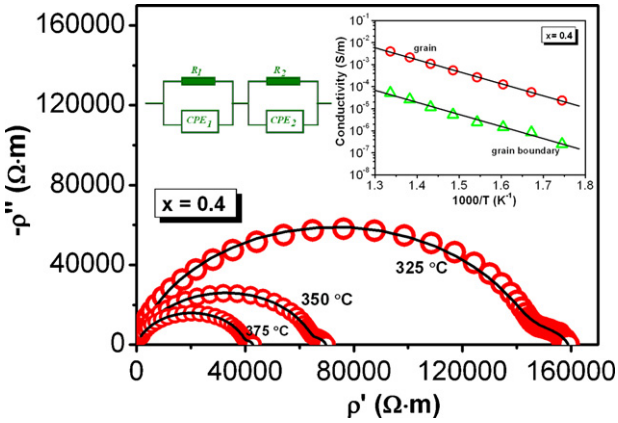

Fig. 2. Typical Nyquist plots of the solid solutions at various temperatures ($x = 0.4$ in this case). The red open circles are experimental values, while the black solid lines are the equivalent circuit fitting results. The inset figure on the top-left is the equivalent circuit, and the top-right inset figure shows the Arrhenius plots of the bulk and grain boundary conductivity.

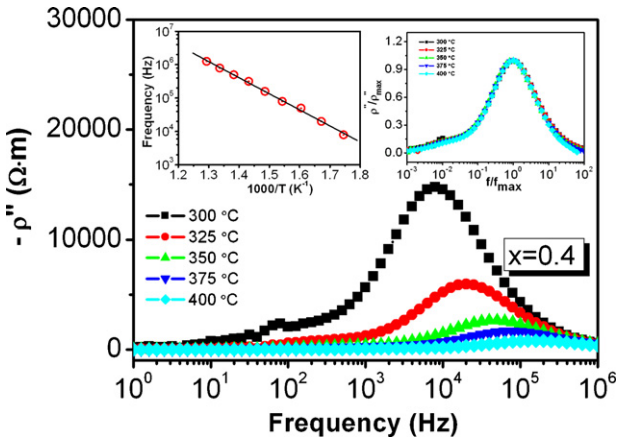

Fig. 3. Bode plots (imaginary impedance vs. frequency) of the solid solution ($x = 0.4$) at various temperatures. The top-left inset figure shows the Arrhenius plot of the bulk relaxation frequency. The top-right inset figure shows the scaling behaviour of the imaginary impedance.

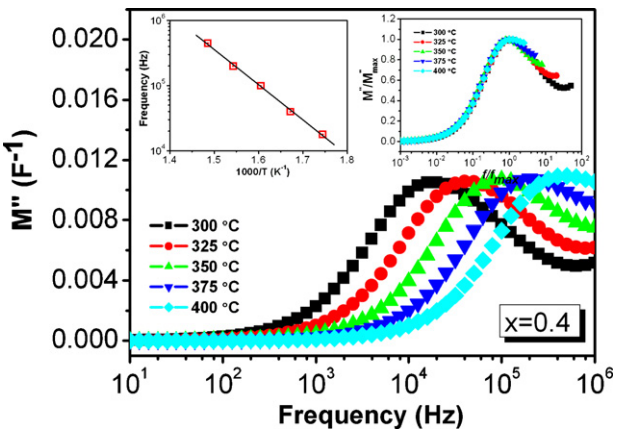

Fig. 4. Frequency dependence of the imaginary electric modulus (M'') of the solid solution ($x = 0.4$) at various temperatures. The top-left inset figure shows the Arrhenius plot of the bulk relaxation frequency. The top-right inset figure shows the scaling behaviour of the imaginary electric modulus.

illustrated by the top-left inset in Fig. 2. The bulk and grain boundary resistances were respectively obtained from the equivalent circuit fitting results and subsequently converted to conductivity by

$$\sigma_{bulk} = \frac{1}{R_{bulk}} \frac{t}{A} \tag{1}$$

and

$$\sigma_{GB}^{sp} = \frac{1}{R_{GB}} \frac{C_{bulk}}{C_{GB}} \frac{t}{A}. \tag{2}$$

The grain boundary conductivity is 2 orders of magnitude lower than the bulk conductivity, which is caused either by the impurity segregation at the grain boundary or the space charge effect due to the oxygen vacancy depletion near the grain boundary region [25]. The temperature dependence of the bulk and the grain boundary conductivity is shown in the top-right inset figure in Fig. 2. Both the bulk and the grain boundary conductivity shows a typical thermally activated process that it increases with an increase in the temperature and its dependence on the temperature obeys the Arrhenius law in the form of

$$\sigma_i = \sigma_{i,0} \exp\left(-\frac{E_{i,a}}{k_B T}\right), \tag{3}$$

where i represents bulk or grain boundary, σ_0 is a pre-exponential factor, k_B is the Boltzmann constant, T is the absolute temperature and E_a is the activation energy. The activation energies can be obtained from the slope of the Arrhenius plots, with values of 1.08 ± 0.01 eV for bulk conduction and 1.09 ± 0.05 eV for grain boundary conduction.

Fig. 3 shows the Bode plots (imaginary impedance vs. frequency) of the selected composition ($x = 0.4$) at various temperatures. The two peaks on the Bode plot correspond to the two semicircles on the Nyquist plot and the peak height is proportional to the resistance of each response (diameter of each semicircle). Because the grain boundary resistance is much smaller than the bulk resistance in this sample (see Fig. 2), the low frequency peak corresponding to the grain boundary response is not obviously distinguished on the Bode plot, but this does not influence the discussion since we mainly focus on the high frequency response (bulk conduction). The frequency at which the peak reaches its maximum is defined as a relaxation frequency ($f_{Z''}$). As shown in thetop-left inset in Fig. 3, the temperature-dependence of $f_{Z''}$ follows the Arrhenius law given by

$$f_{Z''} = f_0 \exp\left(-\frac{E_{Za}}{k_B T}\right), \tag{4}$$

where f_0 is the pre-exponential factor, E_{Za} is the activation energy. The activation energy obtained from $f_{Z''}$ is 1.05 ± 0.02 eV. The top-right inset in Fig. 3 shows the scaling results at different temperatures of the imaginary impedance where ρ''_{max} and $f_{Z'' max}$ are used as the scaling parameters for ρ'' and f, respectively. It can be seen all the imaginary impedance collapses into one master curve, indicating the conduction mechanism remains unchanged within this temperature range [26].

The frequency dependence of the imaginary electric modulus (M'') at various temperatures is shown in Fig. 4. In the modulus plot, only one peak corresponding to the bulk is displayed because of its much smaller capacitance value than that of grain boundary. The peak maximum M''_{max} slightly increases with increasing temperature indicating a weak temperature dependence of the dielectric constant of the sample. Similarly, the relaxation frequency at which the imaginary electric modulus reaches its maximum value, defined as $f_{M''}$, shifts to higher frequency range with increasing temperature, and its temperature-dependence also obeys the Arrhenius law, as shown in the top-left inset of Fig. 4. The activation energy (E_{Ma}) value is 1.07 ± 0.03 eV which is similar to E_{Za}. In a scaled coordinate, as shown in the top-right inset in Fig. 4, all the curves collapse into a single master curve, indicating the relaxation describes the same mechanism at various temperatures [27].

In Fig. 5, the imaginary impedance (ρ'') and the imaginary modulus (M'') were plotted as a function of frequency. The peaks are not overlapped: the peak position for M'' shifts to a higher frequency region compared to the ρ'' peak. According to Ref. [28], the overlapping peak position of imaginary impedance and imaginary modulus is evidence of delocalized or long-range relaxation. Therefore, the slight separation of the two peaks (the peak position of M'' is around half magnitude higher than that of ρ'') suggests the components from both long-range and localized relaxation [29].

3.3. Composition dependence of the bulk conductivity

Fig. 6 shows the composition dependence of the bulk conductivity of the solid solutions at various temperatures. With the increase in the CeO_2 mole ratio, the conductivity first decreases, reaching a minimum around $x = 0.5$, and increases afterward. The "V-shape" variation of the bulk conductivity as a function of the mole ratio of

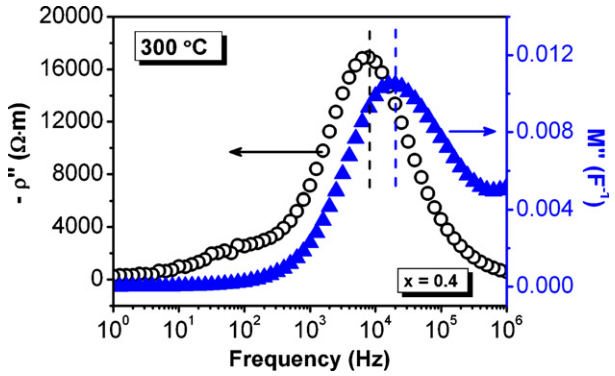

Fig. 5. Frequency dependence of the imaginary impedance (ρ'') and the imaginary electric modulus (M'') of the solid solution ($x = 0.4$) at 300 °C.

CeO_2 indicates that the ternary solid solution deteriorates the electrical conductivity of $(ZrO_2)_{0.92}(Y_2O_3)_{0.08}$ and $(CeO_2)_{0.92}(Y_2O_3)_{0.08}$ binary systems. The inset in Fig. 6 shows the relaxation frequencies obtained from imaginary impedance and imaginary modulus and their dependence on the composition of the solid solutions at a chosen temperature. It is noticeable that $f_{Z''}$ is lower than $f_{M''}$ for all the compositions, indicating the existence of both long-range and localized relaxations in the solid solutions. On the other hand, the composition dependence of $f_{Z''}$ and $f_{M''}$ has a similar trend as the bulk conductivity.

Fig. 7 shows the temperature dependence of the activation energy for the bulk conduction. The activation energy has a decreasing trend, although not linearly, with an increase in x. Slight decrease of the activation energy is observed when $x < 0.5$, while a rapid drop of the activation energy occurs when $x > 0.5$.

4. Discussions

4.1. Relationship between the relaxation frequencies and the conductivity

On the Bode plot (imaginary impedance vs. frequency), a relaxation frequency is obtained where the imaginary impedance reaches its maximum value. In an ideal case of an equivalent circuit of a resistor and a capacitor in parallel connection, the imaginary

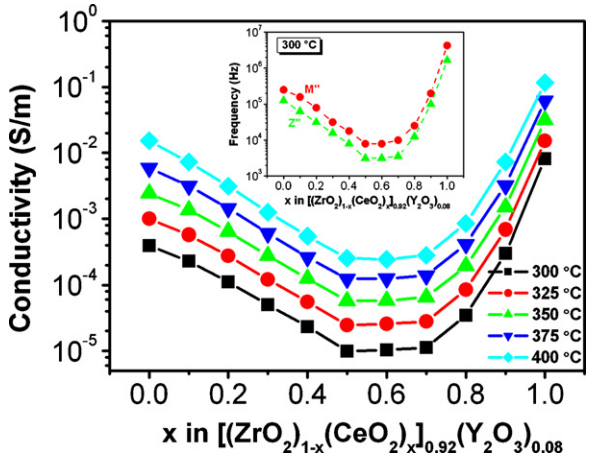

Fig. 6. Composition dependence of the bulk conductivity of the $[(ZrO_2)_{1-x}(CeO_2)_x]_{0.92}(Y_2O_3)_{0.08}$ $(0 \le x \le 1)$ solid solutions at various temperatures. The inset figure shows the composition dependence of relaxation frequencies obtained from imaginary modulus ($f_{M''}$) and imaginary impedance ($f_{Z''}$) at 300 °C.

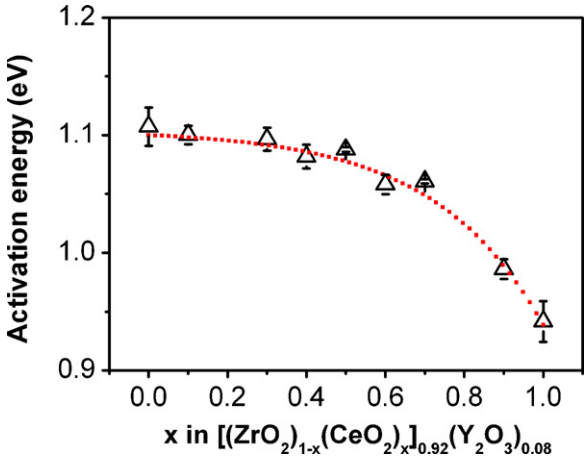

Fig. 7. Composition dependence of the activation energy for the bulk conduction. The hollow triangles are the experimental values obtained from the Arrhenius plot of the bulk conductivity. The red dot is the trend line. (For interpretation of the references to color in this figure caption, the reader is referred to the web version of the article.)

impedance is expressed as:

$$-Z'' = \frac{\omega R^2 C}{1 + \omega^2 R^2 C^2}, \tag{5}$$

where ω is the angular frequency, R is the resistance and C is the capacitance. Maximum of $-Z''$ is obtained when $\omega = 1/RC$. The bulk resistance and capacitance are determined by its conductivity (σ), dielectric constant (ε) and its geometries (t and A as defined in Eq. (2)) by

$$R = \frac{1}{\sigma}\frac{t}{A} \tag{6}$$

and

$$C = \varepsilon\frac{A}{t} \tag{7}$$

Therefore the relaxation frequency $f_{Z''}$ can be expressed by

$$f_{Z''} = \frac{1}{2\pi}\frac{\sigma}{\varepsilon}. \tag{8}$$

In ZrO_2 based ceramics, the dielectric constant is usually insensitive to the composition of the material [30,31] As a result, $f_{Z''}$ is only determined by the conductivity ($f_{M''}$ has the same expression as $f_{Z''}$ in Eq. (8)). A direct proportional relationship can be established between the relaxation frequency and the conductivity.

In the real case, the capacitance response is not a pure capacitor, thus the expression for $f_{Z''}$ will be different from Eq. (8). But for bulk impedance (high frequency response on the Nyquist plot), the deviation from a capacitor is small. Therefore, Eq. (8) can still be used to describe the relationship between $f_{Z''}$ and σ. Comparing the relaxation frequency can be a simple method to rank the bulk conductivity of the solid solutions.

4.2. Origin of the localized relaxation/conduction

When ZrO_2 or CeO_2 is doped with Y_2O_3, oxygen vacancies are generated via the defect reaction:

$$Y_2O_3 \xrightarrow{MO_2} 2Y'_M + V_O^{\bullet\bullet} + 3O_O^x,$$

where M represents Zr or Ce. However, due to the coulomb interaction, some of the oxygen vacancies may bind to the dopant ions and form the defect associates $(Y'_M - V_O^{\bullet\bullet})$. It is usually accepted the orientation of the defect associates under an applied electric field contributes to the localized relaxation [32]. On the other hand, the

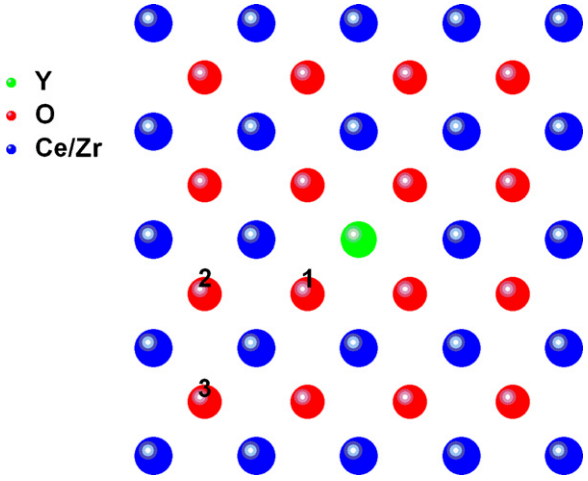

Fig. 8. A schematic top view of the possible sites of oxygen vacancies around a dopant ion. Numbers 1, 2 and 3 represent 1NN, 2NN and 3NN oxygen ions with respect to the dopant (Y) ion.

free oxygen vacancies also contribute to a localized conduction, as discussed below.

The ionic radii of Zr^{4+} and Y^{3+} are 0.084 and 0.1019 nm, respectively [33], while the ionic radius of Ce^{4+} has different reference values, varies from 0.097 [34], 0.101 [35] to 0.110 nm [36]. However, it is clear that the ionic radius of Y^{3+} is close to Ce^{4+} but it is significantly larger than Zr^{4+}. Density functional theoretical studies by Andersson et al. [37] reported that the formation of an anionic vacancy is correlated to the ionic radius of the dopant ion. With respect to the dopant ion, there are three positions, named the first nearest neighbour (1NN), second nearest neighbour (2NN) and third nearest neighbour (3NN), for the oxygen vacancy to locate, as illustrated in Fig. 8. 1NN position is favourable for the oxygen vacancy when the dopant ion has an ionic radius closer to the host cation, and the 2NN position is favourable when the dopant ion has an ionic radius considerably larger than the host cation. Therefore, when Y^{3+} ions substitutes Zr^{4+} ions, oxygen vacancy locates at the 2NN positions (close to Zr centre); when Y^{3+} ions substitutes Ce^{4+} ions, oxygen vacancy locates at the 1NN positions (close to Y centre).

Dholabhai et al. calculated the activation energies for vacancy migration along different paths in praseodymium doped ceria [38] and gadolinium doped ceria [36]. The former can be extended to represent the cases where the ionic radius dopant ion is larger than that of the host ion; while the latter can be extended to represent the case where the ionic radii of the dopant and the host have similar values. According to their calculation results, in both cases the preferred migration pathway for oxygen vacancy diffusion is between 1NN and 2NN sites. For example, in yttria doped ceria, the oxygen vacancy is located at the 1NN position. For migration, it will jump to 2NN position first, and then it is of high possibility that it jumps back to the 1NN site because the jump from 2NN to 1NN has lower activation energy compared with the jumps from 2NN to 2NN or from 2NN to 3NN sites. The back-and-forth jump between two sites contributes to the localized conduction.

In summary, the localized relaxation is from the orientation of the defect associates under the electric field and the back-and-forth jump between two sites of a free oxygen vacancy.

4.3. Composition dependence of the ionic conductivity and the activation energy

In Fig. 6, a "V-shape" variation of the bulk conductivity as a function of x is observed. Similar trend of the composition dependence of the electrical conductivity in ZrO_2–CeO_2–Y_2O_3 solid solutions has been reported by Ananthapadmanabhan et al. [24]. They attributed this V-shape variation to the increased scattering of the oxygen ions by the substitution of Zr by Ce atoms or Ce by Zr atoms, which is analogical to the mechanism of enhanced electrical resistivity in an alloy system. This interpretation is unconvincing to some point that the hopping mechanism in an ionic conductor is totally different from the scattering mechanism of electrons in metals and alloys. Kawamura et al. [20] also found the "V-shape" composition dependence of the conductivity in CaO doped ZrO_2–CeO_2 solid solutions, however they did not give any further explanations on the results. In the following paragraphs the composition dependence of the conductivity will be discussed.

Within the studied temperature range, the electrical conduction in the solid solutions is purely ionic. Therefore, the variation of the bulk conductivity as a function of the composition is either caused by the change of the oxygen vacancy concentration or its mobility. Here we divide the "V-shape" variation as a function of the composition in Fig. 6 into two regions: the CeO_2-rich ($x > 0.5$) and the ZrO_2-rich ($x < 0.5$) regions and discuss them separately.

The increase of the ionic conductivity with the increase of x in the CeO_2-rich region is easier to understand to some extent. In the fluorite structure, the ionic conduction is caused by the migration of oxygen vacancies through channels formed by the neighbouring cations. As discussed by Ananthapadmanabhan et al. [24] and Tsoga et al. [20], the radius of the free channel increases with the lattice parameter. Larger channel radius is favourable for the charge carriers to migrate. Since the amount of Y_2O_3 is set constant for all the compositions, the concentration of oxygen vacancies remains almost the same (the slight increase in the lattice volume leads to a slight decrease of the defect concentration, but this effect is negligible [24]). Therefore, the increase of ionic conductivity in the CeO_2-rich region with increasing x can be attributed to the increased oxygen vacancy mobility through a larger channel.

However, in the ZrO_2-rich region ($x < 0.5$), the increased channel radius fails to explain the decreased ionic conductivity with increasing x. The possible reason for the decreased conductivity in the ZrO_2-rich region with increasing CeO_2 mole ratio is the formation of complex defect associates or clusters. It is well known that 8 mol% YSZ has the highest electrical conductivity. Further increases in dopant concentration decrease the conductivity in YSZ because of the formation of defect associates, which bind the oxygen vacancies to the yttrium ions, making the oxygen vacancies unavailable for conduction [25]. The introduction of CeO_2 into YSZ has similar effect: when CeO_2 is introduced into ZrO_2, additional oxygen vacancies can be generated due to the significant difference of the ionic radius between Ce^{4+} and Zr^{4+} (which is called "size effect") by the following reaction [39]:

$$CeO_2 \xrightarrow{ZrO_2} Ce_{Zr}^{x} + 2V_O^{\bullet\bullet} + 2O_i''.$$

The oxygen vacancies generated by CeO_2 addition makes the formation of $(Y'_{Zr}V_O^{\bullet\bullet})$ becomes more significant, and possibly leads to more complex defect associates $(Y'_{Zr}V_O^{\bullet\bullet}Y'_{Zr})^{x}$, which has been found in 9 mol% Y_2O_3 doped ZrO_2 [40]. The formation of defect associates has stronger effect over the increase in the lattice parameter, and consequently leads to a decreasing conductivity.

To sum up, the "V-shape" variation of the bulk conductivity as a function of x in the solid solutions is a competition between two factors. The first one is the formation of defect associates which limits the mobility of the oxygen vacancies and therefore decreases the conductivity; the second one is the increase of lattice parameter which enlarges the free channel for oxygen vacancy migration and therefore increases the conductivity. In the ZrO_2-rich region ($x < 0.5$), the formation of defect associates overshadows the effect of the increased lattice parameter, therefore the conductiv-

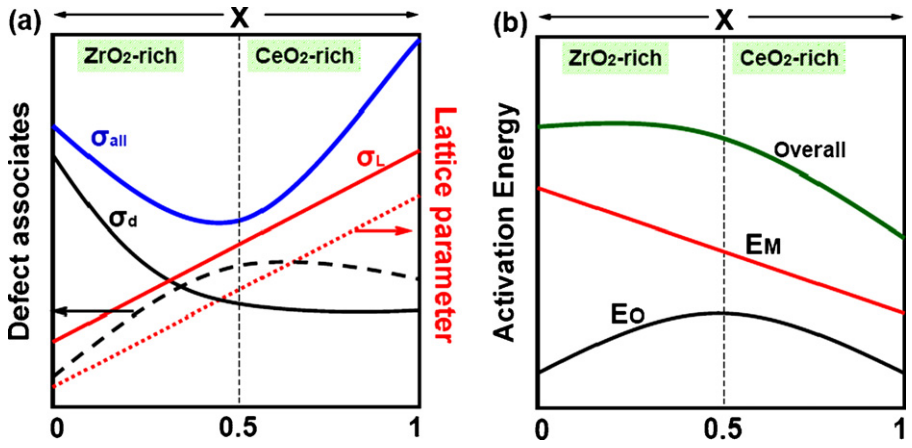

Fig. 9. (a) Schematic of the defect associates profile (black dash line) and lattice parameter (red dot line) as a function of the composition (x). The black solid line illustrates the conductivity decrease caused by increasing defect associates; the red solid line illustrates the conductivity increase due to larger lattice parameter; the blue solid line shows the competitive effect of the two factors on the bulk conductivity of the solid solutions. (b) Schematic of the competitive effect of lattice parameter and the defect associates on the activation energy for the bulk conduction. (For interpretation of the references to color in this figure caption, the reader is referred to the web version of the article.)

ity decreases with increasing x; in the CeO_2-rich region ($x > 0.5$), the increase of lattice parameter is the dominant factor which leads to an up-going trend on the conductivity. A schematic of the defect associates profile and lattice parameter as a function of x and their competitive effect on the bulk conductivity of the solid solutions is shown in Fig. 9(a).

The defect associates and the lattice parameter also influence the activation energy for the bulk conduction, as illustrated in Fig. 9(b). It is accepted that the activation energy for the oxygen diffusion (oxygen vacancy diffusion in an opposite direction) in the intermediate temperature range is comprised of migration energy for a free oxygen vacancy (E_M) and the dissociation energy (E_O) to extricate an oxygen vacancy from the defect associates. As discussed above, the increase of lattice parameter leads to more free space and makes it much easier for an oxygen vacancy to migrate, and therefore a lower E_M. E_O is dependent on the concentration of defect associates. More defect associates, more energy required to dissociate them. Therefore E_O varies as a function of x in the same way as the concentration of defect associates. Since E_M has higher values than E_O [41], in the ZrO_2-rich region, the increased E_O slows down the decrease of E_M, therefore the activation energy shows quite smooth variation; while a rapid drop of the activation energy can be observed in the CeO_2-rich region because E_M and E_O both decrease as a function of x. The experimental observation in Fig. 6 is in agreement with the above analysis.

From the above analysis it can be concluded that the "V-shape" variation of the bulk conductivity with increasing CeO_2 mole ratio is because the ionic radius of Ce^{4+} is significantly larger than Zr^{4+}. Therefore, the ionic radius of the tetravalent dopant determines the composition dependence of the ionic conductivity of the solid solutions. It can be predicted if Zr is substituted by another tetravalent element with the similar ionic radius with Zr^{4+} (e.g., Hf), "V-shape" composition dependence of the bulk conductivity may not be observed.

In order to testify the above prediction, another series of binary solid solution $[(ZrO_2)_{1-x}(HfO_2)_x]_{0.87}(Y_2O_3)_{0.13}$ $(0 \le x \le 0.8)$ has been investigated. The bulk conductivity and the activation energy were obtained using the same method as the ZrO_2–CeO_2–Y_2O_3 series. The ionic radius of Hf^{4+} is 0.083 nm, almost the same as Zr^{4+} (0.084 nm), thus the substitution of Zr^{4+} by Hf^{4+} will not cause the re-arrangement of oxygen vacancies (no "size effect"). Besides at given yttria concentration, yttria-stabilized hafnia has lower ionic conductivity and higher activation energy than YSZ [42], therefore we expect a monotonously decrease of the bulk conductivity, along with a monotonously increase of the activation energy as a function of x. As shown in Fig. 10(a) and (b), both the variations of the bulk conductivity and the activation energy as a function of x are in accordance with the expectations. No "V-shape" composition dependence of the bulk conductivity is observed, which confirms the prediction and from the other side supports the validity of the

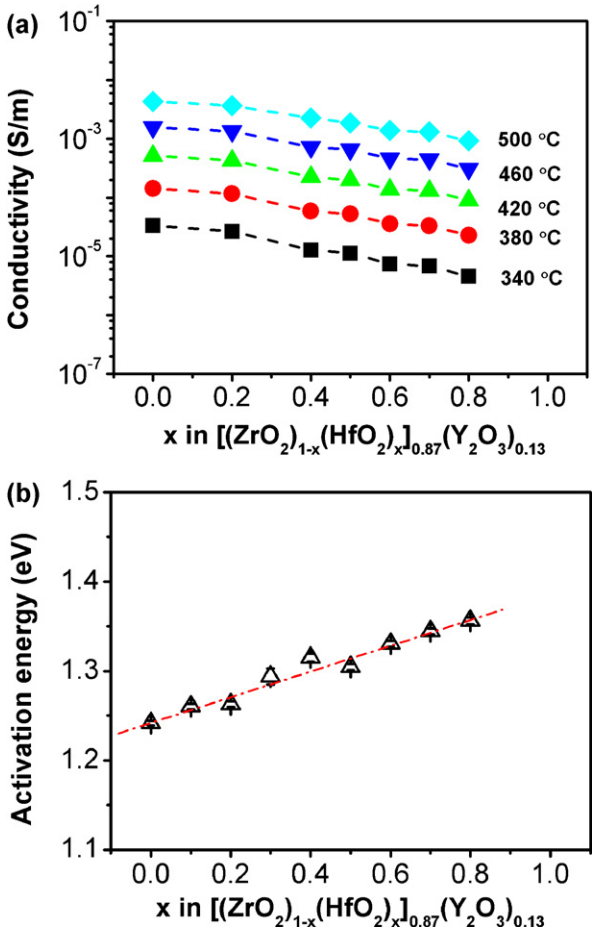

Fig. 10. Composition dependence of (a) bulk conductivity and (b) activation energy of the $[(ZrO_2)_{1-x}(HfO_2)_x]_{0.87}(Y_2O_3)_{0.13}$ $(0 \le x \le 0.8)$ solid solutions at various temperatures.

above explanation of the "V-shape" composition dependence of the bulk conductivity in ZrO_2–CeO_2–Y_2O_3 solid solutions.

5. Conclusions

In this paper, the bulk conduction and relaxation of the $[(ZrO_2)_{1-x}(CeO_2)_x]_{0.92}(Y_2O_3)_{0.08}$ $(0 \le x \le 1)$ solid solutions were studied using impedance spectroscopy at intermediate temperatures (200–500 °C). The main conclusions are: (1) the impedance spectra of the solid solutions of all the compositions show similar characteristic of the well established impedance spectra of YSZ; (2) the relaxation frequency ($f_{Z''}$ and $f_{M''}$) is proportional to the bulk conductivity. Comparing the relaxation frequency can be a simple method to rank the bulk conductivity of the solid solutions; (3) the electrical response of the solid solutions for all the compositions under the ac electrical field shows both long-range and localized relaxations. The localized relaxations are from the orientation of the defect associates under the electric field, as well as the back-and-forth jumping of a free oxygen vacancy between the two sites through which the diffusion path has the lowest activation energy; (4) the bulk conductivity has a "V-shape" variation as a function of the composition: it decreases with an increase of the mole ratio of CeO_2 (x), reaching the lowest value when $x = 0.5$ (Zr/Ce = 1), and then goes up with further increase of x. The decrease of the bulk conductivity with increasing x in the ZrO_2-rich region ($x < 0.5$) is due to the formation of the defect associates which limits the mobility of the oxygen vacancies, while the increase of the bulk conductivity with increasing x in the CeO_2-rich region ($x > 0.5$) is due to the increase of the lattice parameter which enlarges the free channel for oxygen vacancy migration. These two factors also influence the activation energy for the bulk conduction; (5) the ionic radius of the tetravalent dopant determines the composition dependence of the ionic conductivity of the solid solutions. When doping YSZ with other tetravalent dopant with similar ionic radius with Zr^{4+}, e.g., Hf^{4+}, such "V-shape" composition dependence of the bulk conductivity cannot be observed.

References

[1] T. Hibino, A. Hashimoto, T. Inoue, J. Tokuno, S. Yoshida, M. Sano, Science 288 (2000) 2031.
[2] S.C. Singhal, Solid State Ionics 152–153 (2002) 205–410.
[3] W.C. Maskell, Solid State Ionics 134 (2000) 43.
[4] A.Q. Pham, R.S. Glass, Electrochim. Acta 43 (1998) 2699.
[5] J.B. Goodenough, Nature 404 (2000) 821.
[6] K.J. Moreno, A.F. Fuentes, M. Maczka, J. Hanuza, U. Amador, J. Santamaria, C. Leon, Phys. Rev. B 75 (2007) 184303.
[7] S.P.S. Badwal, Solid State Ionics 52 (1992) 23.
[8] O.J. Dura, M.A. Lopez de la Torre, L. Vazquez, J. Chaboy, R. Boada, A. Rivera-Calzada, J. Santamaria nd, C. Leon, Phys. Rev. B 81 (2010) 184301.
[9] X. Guo, R. Yuan, Solid State Ionics 80 (1995) 159.
[10] X. Guo, W. Sigle, J. Fleig, J. Maier, Solid State Ionics 154–155 (2002) 555.
[11] X. Guo, R. Waser, Solid State Ionics 173 (2004) 63–67.
[12] H. Inaba, H. Tagawa, Solid State Ionics 83 (1996) 1.
[13] F. Zhao, A.V. Virkar, J. Power Sources 195 (2010) 6268.
[14] S. Omar, E.D. Wachsman, J.L. Jones, J.C. Nino, J. Am. Ceram. Soc. 92 (2009) 2674.
[15] H. Yamamura, S. Takeda, K. Kakinuma, Solid State Ionics 178 (2007) 1059.
[16] Z.G. Lv, P. Yao, R.S. Guo, F.Y. Dai, Mater. Sci. Eng. A 458 (2007) 355.
[17] B.C.H. Steele, Solid State Ionics 129 (2000) 95.
[18] A. Trovarelli, Catal. Rev. Sci. Eng. 38 (1996) 439.
[19] G.A. Tompsett, N.M. Sammes, J. Am. Ceram. Soc. 80 (1997) 3181.
[20] A. Tsoga, A. Naoumidis, D. Stover, Solid State Ionics 135 (2000) 403.
[21] K. Kawamura, K. Watanabe, T. Hiramatsu, A. Kaimai, Y. Nigara, T. Kawada, J. Mizusaki, Solid State Ionics 144 (2001) 11.
[22] B. Cales, J.F. Baumard, J. Electrochem. Soc. 131 (1994) 2407.
[23] H. Arashi, H. Naito, M. Nakata, Solid State Ionics 76 (1995) 315.
[24] P.V. Ananthapadmanabhan, N. Venkatramani, V.K. Rohatgi, A.C. Momin, K.S. Venkateswarlu, J. Eur. Ceram. Soc. 6 (1990) 111.
[25] X. Guo, R. Waser, Prog. Mater. Sci. 51 (2006) 151.
[26] J. Hou, R. Vaish, Y. Qu, D. Krsmanovic, K.B.R. Varma, R.V. Kumar, J. Power Sources 195 (2010) 2613.
[27] S. Saha, T.P. Sinha, J. Appl. Phys. 99 (2006) 014109.
[28] R. Gerhardt, J. Phys. Chem. Solids 55 (1994) 1491.
[29] A. Dutta, T.P. Sinha, J. Phys. Chem. Solids 67 (2006) 1484.
[30] X. Guo, J. Maier, J. Electrochem. Soc. 148 (2001) 121.
[31] M.C. Steil, F. Thevenot, M. Kleitz, J. Electrochem. Soc. 144 (1997) 390.
[32] H. Yamamura, S. Takeda, K. Kakinuma, Solid State Ionics 178 (2007) 889.
[33] M.R. Winter, D.R. Clarke, Acta Mater. 54 (2006) 5051.
[34] R.D. Shannon, C.T. Prewitt, Acta Crystallogr. B25 (1969) 925.
[35] T.L. Wen, Z.Y. Lu, Z. Xu, J. Mater. Sci. Lett. 13 (1994) 1032.
[36] P.P. Dholabhai, J.B. Adams, P. Crozier, R. Sharma, Phys. Chem. Chem. Phys. 12 (2010) 7904.
[37] D.A. Andersson, S.I. Simak, N.V. Skorodumova, I.A. Abrikosov, B. Johansson, Proc. Natl. Acad. Sci. U.S.A. 103 (2006) 3518.
[38] P.P. Dholabhai, J.B. Adams, P. Crozier, R. Sharama, J. Chem. Phys. 132 (2010) 094104.
[39] J.H. Lee, S.M. Yoon, B.K. Kim, J. Kim, H.W. Lee, H.S. Song, Solid State Ionics 144 (2001) 175.
[40] X. Guo, Z. Wang, J. Eur. Ceram. Soc. 18 (1998) 237.
[41] Y. Arachi, H. Sakai, O. Yamamoto, Y. Takeda, N. Imanishai, Solid State Ionics 121 (1999) 133.
[42] M.F. Trubelja, V.S. Stubican, J. Am. Ceram. Soc. 74 (1991) 2489.